Electrochemistry Communications 13 (2011) 685–688

Contents lists available at ScienceDirect

Electrochemistry Communications

journal homepage: www.elsevier.com/locate/elecom

# Surface states and stability of Fe-containing perovskite electrodes for SOFCs/SOECs by conversion-electron Mössbauer spectroscopy

Ekaterina V. Tsipis [a], João C. Waerenborgh [a], Vladislav V. Kharton [b,*]

[a] Chemistry Department, Instituto Tecnológico e Nuclear, CFMC-UL, EN 10, 2686–953 Sacavém, Portugal
[b] Department of Ceramics and Glass Engineering, CICECO, University of Aveiro, 3810–193 Aveiro, Portugal

ARTICLE INFO

*Article history:*
Received 30 March 2011
Received in revised form 9 April 2011
Accepted 11 April 2011
Available online 17 April 2011

*Keywords:*
Solid oxide fuel cell anode
Steam electrolysis
Perovskite-type oxide electrode
Mg-doped $(La,Sr)(Cr,Fe)O_{3-\delta}$
Redox stability

ABSTRACT

Conversion-electron Mössbauer spectroscopy analysis of model electrochemical cells, comprising porous $^{57}$Fe-enriched $(La_{0.9}Sr_{0.1})_{0.98}Cr_{0.6}Fe_{0.3}Mg_{0.1}O_{3-\delta}$ electrodes and lanthanum gallate solid electrolyte, showed no reductive decomposition of the perovskite electrode material in $H_2$-containing atmosphere at 1073 K, even in the steam electrolysis regime. The predominant state of iron cations in the electrode surface layers was found to remain trivalent irrespective of the oxygen partial pressure in surrounding atmosphere and polarization, whilst oxygen coordination of $Fe^{3+}$ decreases on lowering electrode potential.



## 1. Introduction

Energy-related systems based on solid oxide fuel cells (SOFCs) and electrolysis cells (SOECs) offer important potential advantages due to a high efficiency, environmental safety, fuel flexibility and possibility to recover exhaust heat [1–5]. Significant efforts are focused on the developments of oxide electrode materials stable under both oxidizing and reducing environments, in order to reduce costs of the electrochemical devices and to suppress degradation phenomena, such as coking and sulfur poisoning of the SOFC anodes. These problems are well known for the conventional Ni-containing cermet electrodes, which also degrade owing to large volume changes on redox cycling and sintering during SOFC operation. A very promising combination of properties was recently reported for perovskite-type $(La,Sr)(Cr,Mn)O_{3-\delta}$ (LSCM) [2,3] where the presence of rigid $CrO_6$ octahedra in the crystal structure enables its stabilization down to low oxygen chemical potentials necessary for the SOFC anode operation, whilst moderate acceptor-type doping is necessary to improve electronic and ionic transport. The incorporation of iron in $LaCrO_3$ may further enhance electrode performance [3,4]. However, information on phase stability of $(La,Sr)(Cr,Fe)O_{3-\delta}$ in reducing atmospheres is still quite contradictory [3–6]. Moreover, no data on surface states in these perovskite electrodes under reducing conditions are available up to now, although the surface defects and oxygen deficiency level are critically important for the electrochemical and catalytic activity [7–9]. It should also be mentioned that under high current densities, the oxygen chemical potentials at an electrode surface and electrode/electrolyte interface differ substantially from the surrounding gaseous phase [1,7], thus raising additional requirements to the redox and dimensional stability of the electrode materials.

The present work was centered on the analysis of iron oxidation states and coordination in the surface and near-surface layers of model $^{57}$Fe-enriched $(La_{0.9}Sr_{0.1})_{0.98}Cr_{0.6}Fe_{0.3}Mg_{0.1}O_{3-\delta}$ electrodes by conversion-electron Mössbauer spectroscopy (CEMS). To authors' knowledge, the CEMS technique is used in this area of solid state electrochemistry for the first time. Although CEMS is a highly-selective and non-destructive method advantageous to study interfacial phenomena, its applications to bulky complex materials are rare as it requires large concentrations of $^{57}$Fe isotope on and near the surface (e.g. [10] and references cited). For recording the spectra, the $^{57}$Fe concentration in the subsurface layers should be at least ~$10^{14}$ atoms/cm$^2$, while the natural abundance of $^{57}$Fe is only 2.2 at.% [10]. Hence, the conversion-electron Mössbauer (CEM) spectra are usually collected for iron-rich compositions, for $^{57}$Fe-doped thin films, or when $^{57}$Fe is implanted into surfaces. The maximum depth analyzed by integral CEMS registering all electrons back-scattered from the surface is approximately 200–300 nm [10]. In this work, $^{57}$Fe-enriched perovskite $(La_{0.9}Sr_{0.1})_{0.98}Cr_{0.6}Fe_{0.3}Mg_{0.1}O_{3-\delta}$ was selected as a model electrode material with relatively high concentration of iron and moderate content of acceptor-type dopants, $Sr^{2+}$ and $Mg^{2+}$; further substitution is expected to significantly decrease thermodynamic stability of the perovskite-type solid solution [5]. The CEM spectra of porous $(La_{0.9}Sr_{0.1})_{0.98}Cr_{0.6}Fe_{0.3}Mg_{0.1}O_{3-\delta}$ electrodes are

* Corresponding author. Tel.: +351 234 370263; fax: +351 234 425300.
*E-mail address:* kharton@ua.pt (V.V. Kharton).

1388-2481/$ – see front matter © 2011 Elsevier B.V. All rights reserved.
doi:10.1016/j.elecom.2011.04.009

compared to the results of transmission Mössbauer spectroscopy (TMS), collected using powdered samples equilibrated in various atmospheres.

## 2. Experimental

The experimental conditions used in this work for the electrode preparation and characterization were similar to those described earlier for LSCM anodes [11]. Single-phase $(La_{0.9}Sr_{0.1})_{0.98}Cr_{0.6}{}^{57}Fe_{0.3}Mg_{0.1}O_{3-\delta}$ powder was synthesized by the glycine–nitrate process (GNP). Prior to the synthesis, the stoichiometric amount of metallic iron enriched with $^{57}Fe$ isotope (95.7%, Chemgas, France) was dissolved in diluted nitric acid and then added into the solution used for the GNP. The obtained powders were annealed at 1273–1473 K in air for 12 h with several intermediate regrinding steps. Phase purity was confirmed by X-ray diffraction (XRD), Fig. 1. The porous electrode layers were screen-printed onto dense solid-electrolyte membranes of $(La_{0.9}Sr_{0.1})_{0.98}Ga_{0.8}Mg_{0.2}O_{3-\delta}$ (LSGM) tested elsewhere [12], and were sintered in air at 1473 K for 2 h. Examination by scanning electron microscopy (SEM) revealed the formation of homogeneous electrode microstructure with a high porosity and submicron grain size, which was essentially unchanged during polarization tests. Typical SEM micrographs are presented in the inset of Fig. 1. The area, thickness and sheet density of the working electrodes were $1.44 \pm 0.01$ cm$^2$, $52 \pm 6$ μm and $16 \pm 2$ mg/cm$^2$, respectively; the electrolyte membrane thickness was $1.35 \pm 0.01$ mm. The counter electrodes made of porous Pt were applied onto the opposite side of LSGM and sintered in air at 1273 K for 0.5 h. The model electrochemical cells were placed at 1073 K in flowing wet 10% $H_2$–90% $N_2$ gas mixture where the oxygen partial pressure, $p(O_2)$, was continuously monitored by an electrochemical oxygen sensor. In this work, $p(O_2)$ was fixed equal to $1 \times 10^{-20}$ atm at 1073 K in all cases. After equilibration, DC voltage ($U$) of +1.1, 0 or −1.1 V was applied to the cell electrodes during 24 h. Following fast cooling (8–12 K/min) under the applied DC voltage, the electrochemical cells were analyzed by CEMS and SEM/EDS. For the sake of comparison, a series of powdered samples of $(La_{0.9}Sr_{0.1})_{0.98}Cr_{0.6}Fe_{0.3}Mg_{0.1}O_{3-\delta}$ were annealed in the same atmosphere at 1023–1223 K during 24 h and then studied by XRD and TMS. The equipment and experimental procedures used for XRD, TMS and SEM/EDS were described elsewhere [9,11–13]. CEMS was performed at room temperature, with the samples mounted inside a

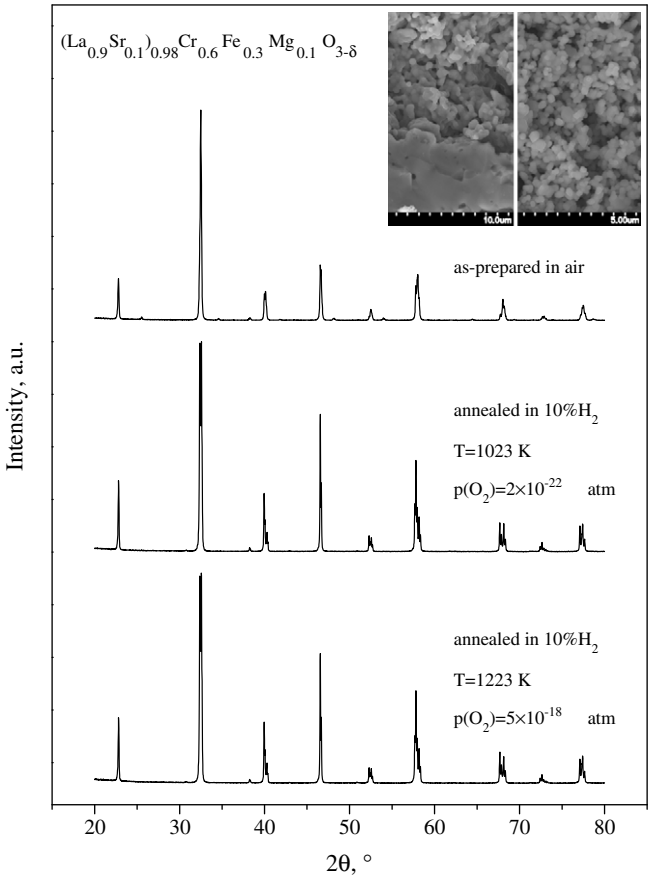


**Fig. 1.** XRD patterns of $^{57}Fe$-enriched $(La_{0.9}Sr_{0.1})_{0.98}Cr_{0.6}Fe_{0.3}Mg_{0.1}O_{3-\delta}$ after synthesis in air, and after annealing in flowing 10%$H_2$–90%$N_2$ gas mixture at $T = 1023$–1223 K. Inset shows the SEM micrographs of fractured electrochemical cells with $(La_{0.9}Sr_{0.1})_{0.98}Cr_{0.6}{}^{57}Fe_{0.3}Mg_{0.1}O_{3-\delta}$ electrode and LSGM electrolyte (left), and top-view of the electrode layer (right) after anodic polarization in 10%$H_2$–90%$N_2$ at 1073 K for 24 h.

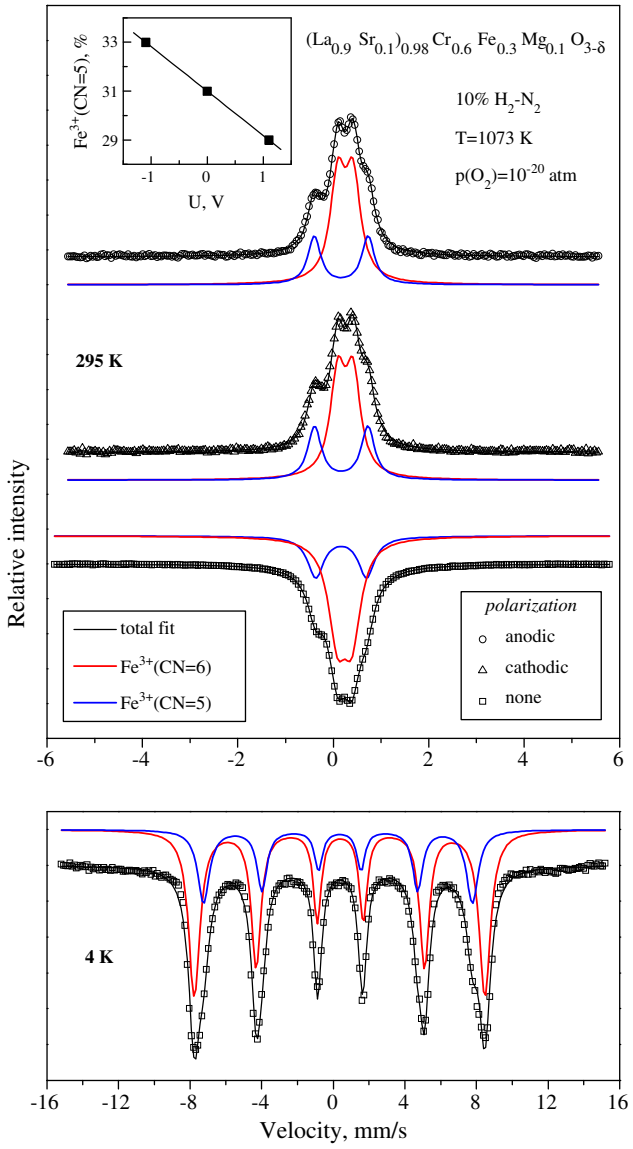


**Fig. 2.** Comparison of the room-temperature CEM spectra of porous $(La_{0.9}Sr_{0.1})_{0.98}Cr_{0.6}{}^{57}Fe_{0.3}Mg_{0.1}O_{3-\delta}$ electrodes in contact with LSGM solid electrolyte after polarization (top), and room-temperature and 4 K TM spectra of $(La_{0.9}Sr_{0.1})_{0.98}Cr_{0.6}{}^{57}Fe_{0.3}Mg_{0.1}O_{3-\delta}$ powder equilibrated in the same environment (bottom). The lines plotted over the experimental points are the sum of two quadrupole doublets or magnetic sextets, shown shifted for clarity. The anodic ($U = +1.1$ V) and cathodic ($U = -1.1$ V) polarization tests were performed in flowing 10%$H_2$–90%$N_2$ at $T = 1073$ K and $p(O_2) = 10^{-20}$ atm for 24 h. Inset shows the fraction of penta-coordinated $Fe^{3+}$ vs. voltage applied to the electrochemical cells.

proportional backscatter detector RIKON-5 (Wissel) in a flowing 5% $CH_4$–95% He gas mixture. The CEM and transmission Mössbauer (TM) spectra were fitted to Lorentzian lines using a non-linear least-squares method. In the course of refinement, the relative areas and line widths of both peaks in a quadrupole doublet and peaks 1–6, 2–5 and 3–4 in a magnetic sextet were constrained equal. The functional properties of $(La_{0.9}Sr_{0.1})_{0.98}Cr_{0.6}Fe_{0.3}Mg_{0.1}O_{3-\delta}$ ceramics and electrodes, including the total conductivity, thermal and chemical expansion, oxygen permeability and polarization resistance, will be reported in a separate publication.

## 3. Results and discussion

Fig. 2 compares the CEM and TM spectra of porous $(La_{0.9}Sr_{0.1})_{0.98}Cr_{0.6}{}^{57}Fe_{0.3}Mg_{0.1}O_{3-\delta}$ electrodes after cathodic and anodic polarization tests in wet 10% $H_2$–90% $N_2$ during 24 h, and powders of the same composition equilibrated in reducing and oxidizing atmospheres. The room-temperature and 4.2 K TM spectra of the reduced powder annealed at $p(O_2)=10^{-20}$ atm and 1073 K, consist of two quadrupole doublets and two magnetic sextets, respectively (Fig. 2, bottom). These two subspectra clearly indicate the presence of $Fe^{3+}$ cations with 6- and 5-fold oxygen coordination (Table 1), with considerably higher isomer shifts (IS) than those typical for tetrahedral $Fe^{3+}$, 0.14–0.22 mm/s at room temperature [13–15]. In addition to lower IS values, the signal of penta-coordinated $Fe^{3+}$ has higher quadrupole splitting (QS) as expected for a site with more distorted coordination polyhedra compared to the iron–oxygen octahedra. The TM spectra of the oxidized perovskite phase equilibrated with atmospheric oxygen show that the octahedrally-coordinated $Fe^{3+}$ state is predominant (Table 1). Moreover, neither $Fe^{2+}$, $Fe^{4+}$ nor tetrahedrally-coordinated $Fe^{3+}$ can be detected in the reduced and oxidized powders. Notice that, due to the significantly lower IS and magnetic hyperfine fields of 4-fold coordinated $Fe^{3+}$, at least the peaks located at the highest Doppler velocity of the corresponding sextets should be resolved at 4.2 K if the $Fe^{3+}O_4$ tetrahedra were present [9,14,15]. The observed behavior shows hence that the oxygen vacancies formed on reduction of $(La_{0.9}Sr_{0.1})_{0.98}Cr_{0.6}{}^{57}Fe_{0.3}Mg_{0.1}O_{3-\delta}$ are statistically distributed in the lattice, whereas the oxidation state of iron cations in this perovskite is essentially independent of the oxygen nonstoichiometry and remains 3+ within the limits of experimental uncertainty. The latter means, in particular, that the vacancy formation is charge-compensated by $Cr^{3+}/Cr^{4+}$ redox couple. This trend is opposite with respect to $La_{1-x}Sr_xCr_{0.5}Mn_{0.5}O_{3\pm\delta}$ series [16] where X-ray absorption spectroscopy indicated an essentially constant state of $Cr^{3+}$ cations.

Irrespective of the electronic subsystem, the absence of peaks characteristic of $Fe^{2+}$ and metallic Fe in the TM spectra of reduced $(La_{0.9}Sr_{0.1})_{0.98}Cr_{0.6}{}^{57}Fe_{0.3}Mg_{0.1}O_{3-\delta}$ (Fig. 2) confirms that the perovskite phase is preserved at $p(O_2)=10^{-20}$ atm and 1073 K. This conclusion is in agreement with the XRD results (Fig. 1) indicating that no extra phases appear on reduction. Decreasing $p(O_2)$ leads to a transition from orthorhombic (space group *Pnma*) to rhombohedrally distorted perovskite structure (S.G. $R\bar{3}c$), as reported earlier for $La_{0.75}Sr_{0.25}Cr_{0.5}Fe_{0.5}O_{3-\delta}$ [8], and to a moderate lattice expansion due to the oxygen vacancy formation. For example, the unit cell parameters of oxidized $(La_{0.9}Sr_{0.1})_{0.98}Cr_{0.6}Fe_{0.3}Mg_{0.1}O_{3-\delta}$, calculated from the room-temperature XRD patterns, were: $a=5.5063(2)$ Å, $b=5.5156(2)$ Å, $c=7.7976(4)$ Å, $V=236.82(2)$ Å$^3$. After reduction at 1223 K and $p(O_2)=5\times10^{-18}$ atm, the rhombohedral lattice parameters expressed in hexagonal settings were: $a=5.5363(1)$ Å, $c=13.4484(3)$ Å, $V=356.97(1)$ Å$^3$. The increase in the unit cell volume ($V$) normalized to orthorhombic perovskite, 0.49%, is comparable to analogous results on $La_{0.75}Sr_{0.25}Cr_{0.5}Fe_{0.5}O_{3-\delta}$, 0.31% [8]. Taking into account the TMS data, this volume increment is essentially contributed by increasing radius of chromium cations when their oxidation state decreases.

As for TMS, the room-temperature CEM spectra of the porous electrodes, collected after the polarization tests in flowing 10%$H_2$–90% $N_2$ at 1073 K, exhibit only two doublets corresponding to hexa- and penta-coordinated $Fe^{3+}$ (Fig. 2 and Table 1). Again, no traces of metallic Fe and $Fe^{2+}$ states are visible, even after cathodic polarization ($U=-1.1$ V). The latter regime corresponds to the water vapor electrolysis, when the oxygen chemical potential at the electrode is much lower than that in the supplied gas flow, $p(O_2)=10^{-20}$ atm. Under anodic polarization ($U=+1.1$ V), this chemical potential is higher as oxygen is pumped through the solid electrolyte membrane onto the working electrode. The fraction of penta-coordinated $Fe^{3+}$ was found to exhibit a linear dependence on the applied voltage (inset in Fig. 2), reflecting the oxygen deficiency variations induced by the electrode polarization. The changes in $Fe^{3+}$ (CN = 5) concentration with respect to the equilibrium conditions are relatively small but statistically significant (Table 1).

In summary, the results demonstrate that CEMS is sensitive enough to the local alterations of oxygen nonstoichiometry in the Fe-containing electrode surface layers under polarization. This makes it possible, in particular, to experimentally study the oxygen chemical potential distribution across electrode bulk and current-dependent defect chemistry in porous electrodes by the differential CEMS enabling to collect signals from different depths, and/or by combining layer-by-layer polishing of the electrode layers and integral CEMS technique. The CEMS and TMS analyses of the model electrochemical cells with $(La_{0.9}Sr_{0.1})_{0.98}Cr_{0.6}{}^{57}Fe_{0.3}Mg_{0.1}O_{3-\delta}$ layers show also that the trivalent state of iron cations remains essentially unchanged under reducing conditions, even in the steam electrolysis regime.

**Table 1**
Parameters[a] estimated from the CEM spectra of $(La_{0.9}Sr_{0.1})_{0.98}Cr_{0.6}{}^{57}Fe_{0.3}Mg_{0.1}O_{3-\delta}$ electrodes after polarization tests in flowing 10%$H_2$–90%$N_2$ at 1073 K, and TM spectra of the powders equilibrated in the same atmosphere and in atmospheric air.

| Conditions | Technique | $T$, K | IS, mm/s | QS, mm/s | 2ε, mm/s | $B_{hf}$, T | CN | $I$, % |
|---|---|---|---|---|---|---|---|---|
| Equilibration | TMS | 295 | 0.36 | 0.38 | | – | 6 | 100 |
| in air at 295 K | | 4 | 0.49[b] | | −0.05 | 47.2 [b] | 6 | 100 |
| Equilibration | TMS | 295 | 0.35 | 0.31 | | – | 6 | 70 |
| in 10% $H_2$ at 1073 K | | | 0.28 | 1.06 | | – | 5 | 30 |
| | | 4 | 0.49 | | −0.04 | 50.3 | 6 | 69 |
| | | | 0.43 | | −0.10 | 46.6 | 5 | 31 |
| Anodic polarization | CEMS | 295 | 0.37 | 0.32 | | – | 6 | 71 |
| in 10% $H_2$ at 1073 K | | | 0.28 | 1.13 | | – | 5 | 29 |
| Cathodic polarization | CEMS | 295 | 0.37 | 0.32 | | – | 6 | 67 |
| in 10% $H_2$ at 1073 K | | | 0.28 | 1.12 | | – | 5 | 33 |

[a] IS, QS, $2\varepsilon=(e^2V_{ZZ}Q/4)(3\cos^2\theta-1)$, $B_{hf}$, $I$ and CN are the isomer shift relative to metallic α-Fe at 295 K, quadruple splitting, quadruple shift, magnetic hyperfine field, relative area and oxygen coordination number, respectively. Estimated errors are ≤0.2 T for $B_{hf}$, ≤1% for $I$, and ≤0.02 mm/s for the other parameters.
[b] Average values of a magnetic sextet distribution.

Although long-term electrochemical testing in pure $H_2$–$H_2O$, CO–$CO_2$ and converted $CH_4$ atmospheres is necessary, the data obtained in this work suggest that Fe-substituted chromites and their derivatives may provide a stable operation of intermediate-temperature SOFC anodes.

## Acknowledgements

This work was supported by the FCT, Portugal (projects PTDC/CTM/64357/2006, PTDC/CTM-CER/114561/2009 and SFRH/BPD/28629/2006).

## References

[1] V. Kharton (Ed.), Solid State Electrochemistry I: Fundamentals, Materials and their Applications, Wiley-VCH, Weinheim, 2009.
[2] S. Tao, J.T.S. Irvine, Nat. Mater. 2 (2003) 320.
[3] J. Peña-Martínez, D. Marrero-López, D. Pérez-Coll, J.C. Ruiz-Morales, P. Núñez, Electrochim. Acta 52 (2007) 2950.
[4] J.M. Haag, B.D. Madsen, S.A. Barnett, K.R. Poeppelmeier, Electrochem. Solid State Lett. 11 (2008) B51.
[5] J. Sfeir, J. Power Sources 118 (2003) 276.
[6] M. Oishi, K. Yashiro, K. Sato, J. Mizusaki, T. Kawada, J. Solid State Chem. 181 (2008) 3177.
[7] M.K. Bruce, M. van den Bossche, S. McIntosh, J. Electrochem. Soc. 155 (2008) B1202.
[8] S. Tao, J.T.S. Irvine, Chem. Mater. 16 (2004) 4116.
[9] V.V. Kharton, M.V. Patrakeev, J.C. Waerenborgh, V.A. Sobyanin, S.A. Veniaminov, A. A. Yaremchenko, P. Gaczyński, V.D. Belyaev, G.L. Semin, J.R. Frade, Solid State Sci. 7 (2005) 1344.
[10] M. Seberíni, J. Sitek, J. Electr. Eng. 59 (2008) 234.
[11] V.V. Kharton, E.V. Tsipis, I.P. Marozau, A.P. Viskup, J.R. Frade, J.T.S. Irvine, Solid State Ionics 178 (2007) 101.
[12] V.V. Kharton, A.L. Shaula, N.P. Vyshatko, F.M.B. Marques, Electrochim. Acta 48 (2003) 1817.
[13] V.V. Kharton, A.V. Kovalevsky, M.V. Patrakeev, E.V. Tsipis, A.P. Viskup, V.A. Kolotygin, A.A. Yaremchenko, A.L. Shaula, E.A. Kiselev, J.C. Waerenborgh, Chem. Mater. 20 (2008) 6457.
[14] P.D. Battle, T.C. Gibb, S. Nixon, J. Solid State Chem. 79 (1989) 75.
[15] P. Adler, U. Schwarz, K. Syassen, A.P. Milner, M.P. Pasternak, M. Hanfland, J. Solid State Chem. 155 (2000) 381.
[16] S.M. Plint, P.A. Connor, S. Tao, J.T.S. Irvine, Solid State Ionics 177 (2006) 2005.